analytical chemistry

Article

pubs.acs.org/ac

Selective Tracking of Lysosomal Cu^{2+} Ions Using Simultaneous Target- and Location-Activated Fluorescent Nanoprobes

Yinhui Li,[†,§] Yirong Zhao,[†,§] Winghong Chan,[‡] Yijun Wang,[†] Qihua You,[‡] Changhui Liu,[†] Jing Zheng,[†] Jishan Li,[†] Sheng Yang,[†] and Ronghua Yang*[,†]

[†]State Key Laboratory of Chemo/Biosensing and Chemometrics, College of Chemistry and Chemical Engineering, Collaborative Innovation Center for Chemistry and Molecular Medicine, Hunan University, Changsha, 410082, China

[‡]Department of Chemistry, Hong Kong Baptist University, Kowloon Tong, Kowloon, Hong Kong, China

Supporting Information

ABSTRACT: Levels of lysosomal copper are tightly regulated in the human body. However, few methods for monitoring dynamic changes in copper pools are available, thus limiting the ability to diagnostically assess the influence of copper accumulation on health status. We herein report the development of a dual target and location-activated rhodamine−spiropyran probe, termed Rhod-SP, activated by the presence of lysosomal Cu^{2+}. Rhod-SP contains a proton recognition unit of spiropyran, which provides molecular switching capability, and a latent rhodamine fluorophore for signal transduction. Upon activation by lysosomal acidic pH, Rhod-SP binds with Cu^{2+} by spiropyran-based proton activation, promoting, in turn, rhodamine ring opening, which shows a "switched on" fluorescence signal. However, to protect Rhod-SP from degradation and interference by the physiological environment, it is engineered on mesoporous silica nanoparticles (MSNs), and the surface of Rhod-SP@MSNs is further anchored with β-cyclodextrin (β-CD) to enhance the solubility and bioavailability of Rhod-SP@MSN-CD. Next, to enhance cell specificity, a guiding unit of c(RGDyK) peptide conjugated adamantane (Ad-RGD) as prototypical system, is incorporated on the surface of Rhod-SP@MSN-CD to target integrin $\alpha_v\beta_3$ and $\alpha_v\beta_5$ overexpressed on cancer cells. Fluorescence imaging showed that both Rhod-SP@MSN-CD and Rhod-SP@MSN-CD-RGD were suitable for visualizing exogenous and endogenous Cu^{2+} in lysosomes of living cells. This strategy addresses some common challenges of chemical probes in biosensing, such as spatial resolution in cell imaging, the solubility and stability in biological system, and the interference from intracellular species. The newly designed nanoprobe, which allows one to track, on a location-specific basis, and visualize lysosomal Cu^{2+}, offers a potentially rich opportunity to examine copper physiology in both healthy and diseased states.

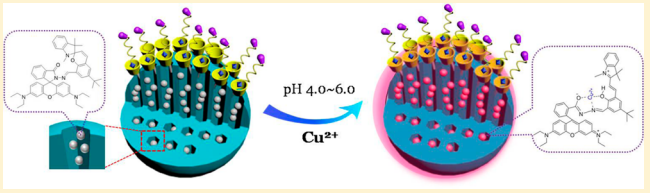

Copper plays a crucial role in many cellular processes, and its concentration at the cellular level is related to severe physiological and pathological events.[1−3] Because of its essential, yet toxic, nature, intracellular copper distribution is strictly controlled by cells. It has been demonstrated that some human copper transporters localize late in endosomes and lysosomes to facilitate cellular copper uptake.[4−6] However, excess copper excreted from cytoplasm can accumulate in lysosomes, causing a highly toxic state and resulting in serious infant liver damage, such as Wilson's disease.[7,8] On the other hand, the loss of copper homeostasis can result in Alzheimer's disease and Menkes disease.[9,10] Therefore, it is desirable to develop new molecular tools to monitor lysosomal copper concentrations.

While numerous molecular tools for intracellular Cu^{2+} have been developed and applied to intracellular imaging,[11−15] of which capability to selective track the metal in an organelle have been rarely reported.[16−18] In the seminal work of Chang et al., a targetable fluorescent probe for imaging exchangeable mitochondrial Cu^{+} pools was recently proposed.[16] The probe was chemically designed by combining a Cu^{+} responsive fluorescent platform with a mitochondrial-targeting triphenylphosphonium moiety for localizing the probe to the organelle.[19,20] However, the imperfect targeting ability of these guidance systems, along with the nonspecific distribution of the analyte throughout the cell, resulted in considerable background signal from cytosol and other organelles, making it impossible to achieve high resolution at the suborganelle level. In addition, the poor solubility of the probe molecules, combined with the degradation of the molecules by lysosomal acid and hydrolase,[21,22] as well as interference from other intracellular species, have remained challenging. Nonetheless, we have been committed to solving these problems within the context of our ongoing interest in developing highly sensitive and selective spiropyran-based molecular probes.[23−25] As a consequence of our efforts, we proposed herein a new strategy for real-time targeting and selective tracking of lysosomal Cu^{2+} ions. The new designed fluorescent spiropyran-based probe,

Received: August 26, 2014
Accepted: December 1, 2014

   dx.doi.org/10.1021/ac503240x | *Anal. Chem.* XXXX, XXX, XXX−XXX

termed Rhod-SP, which contains an proton recognition unit of spiropyran and a latent Cu^{2+}-complexed rhodamine fluorophore, allows tracking on a location-specific basis and visualizing lysosomal Cu^{2+}.

To ensure that Rhod-SP can most accumulate in lysosomes and efficiently track Cu^{2+} without deleterious interference from biological systems, we chose mesoporous silica nanoparticles (MSNs) as the probe reservoir, a familiar nanocarrier, and lysosomal marker.[26−30] The surface of Rhod-SP@MSNs was then anchored with β-cyclodextrin (β-CD) as a gatekeeper, to eliminate interference from intracellular species, but allow Cu^{2+} ions to enter the nanopores and react with Rhod-SP. To enhance cell specificity, a c(RGDyK) peptide conjugated with adamantane (Ad-RGD) was incorporated on the surface of Rhod-SP@MSN-CD to target integrin $\alpha_v\beta_3$ and $\alpha_v\beta_5$ overexpressed on cancer cells,[31] resulting in Rhod-SP@MSN-CD-RGD that targets lysosomal Cu^{2+} via the specific recognition of integrin $\alpha_v\beta_3$ and $\alpha_v\beta_5$ overexpressed in cancer cells. On the basis of these strategies, the ability to monitor the dynamics of lysosomal copper at high spatial resolution offers a potentially rich opportunity to examine copper physiology in both healthy and diseased states.

EXPERIMENTAL SECTION

Preparation of Rhod-SP-Based Nanoprobes. *Synthesis of Rhod-SP.* The synthesis route of Rhod-SP is shown in Scheme 1A (for details, see Supporting Information). Compound **1** was obtained via the Duff reaction by using anhydrous trifluoroacetic acid, and the reaction of Rhodamine B with hydrazine hydrate afforded compound **2**. Then, compounds **1** and **2** were mixed at room temperature and stirred for 12 h, giving compound **3**. Finally, Rhod-SP was obtained via Knoevenagel condensation reaction of compound **3** and 1,2,3,3-tetramethyl-3H-indolium in 75% yield.

Preparation of Rhod-SP@MSN-CD and Rhod-SP@MSN-CD-RGD. MSN-NH_2 was prepared according to a protocol given in the literature.[32] Briefly, purified MSN-NH_2 (10 mg) was added to an acetonitrile solution (5 mL) of Rhod-SP (20 mM). The solution mixture was stirred at room temperature for 24 h, to allow encapsulation of Rhod-SP by MSN-NH_2. The resulting particles were then separated by centrifugation and dispersed in a mixture solution (dimethyl sulfoxide/water (DMSO/H_2O) = 1:1, v/v) with mono-6-deoxy-6-(*p*-tolylsulfonyl)-β-cyclodextrin (6-OTs-β-CD) (90 mg). The mixture was allowed to react for 24 h at 45 °C under nitrogen atmosphere to yield Rhod-SP@MSN-CD. The resulting material was filtered and extensively washed with ultrapure water and ethanol and dried under high vacuum at 60 °C. To modify the RGD to Rhod-SP@MSN-CD, Rhod-SP@MSN-CD (1.0 mg) and adamantine-functionalized RGD (0.2 mg) were added to 1.0 mL of ultrapure water. The mixture reacted for 0.5 h at room temperature. After the reaction, Rhod-SP@MSN-CD-RGD complexes were washed three times by centrifugation at 14 000 rpm with ultrapure water.

Spectrophotometric Measurements. Both fluorescence and UV-vis absorption measurements of Rhod-SP@MSN-CD were conducted in sodium acetate/acetic acid buffer solution. For Cu^{2+} assay, 1.0 mL sodium acetate/acetic acid buffer (20 mM, pH 5.0) containing 1.0 μM Rhod-SP or 50 μg/mL Rhod-SP@MSN-CD was first introduced to a quartz cell. Following the additions of different concentration of Cu^{2+} solution, the fluorescence intensities were recorded at excitation wavelength of 550 nm with an emission wavelength range from 540 nm to 700 nm.

Scheme 1. (A) Synthetic Route for Rhod-SP. (B) Proposed Scheme of Fluorescence Response of Rhod-SP by Binding of H^+ and Cu^{2+}

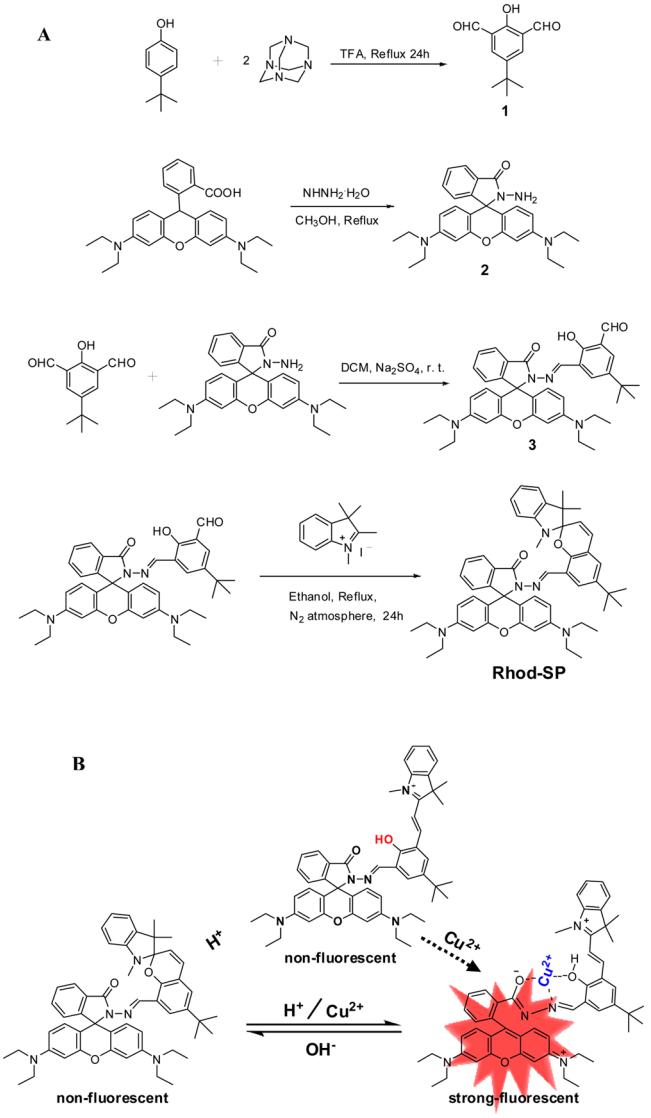

To measure leakage of Rhod-SP from MSNs, Rhod-SP@MSN and Rhod-SP@MSN-CD were suspended in 300 μL of buffer solution, respectively, sealed in a homemade dialysis tube with a molecular weight cutoff of 8000−14 000 Da, and then immersed in 1.7 mL of buffer solution containing 10.0 μM Cu^{2+} at 37 °C. The system was moderately shaken. The fluorescence intensity of dialysis fluid was measured at certain time points with an excitation wavelength of 550 nm.

Cell Imaging. HeLa cells were incubated with 50 μg/mL Rhod-SP@MSN-CD for 3.0 h in the culture medium, followed by supplementation with 50 μM $CuCl_2$ for 12.0 h. Cells were also treated with EDTA before and after incubation with Rhod-SP@MSN-CD for 2.0 h, respectively. In addition, after cells were supplemented with $CuCl_2$ and incubated with Rhod-SP@MSN-CD, 1,8-bis(dimethylamino)naphthalene (DMAN), a common proton sponge, was further incubated with cells for 2.0 h to promote lysosomal damage. Cells were washed three times with PBS and then analyzed by confocal fluorescence

dx.doi.org/10.1021/ac503240x | Anal. Chem. XXXX, XXX, XXX−XXX

microscopy. To monitor exogenous Cu^{2+} in cells, the cells were pretreated with different concentrations of $CuCl_2$ solution for 12.0 h and then incubated with 50 μg/mL Rhod-SP@MSN-CD for 3.0 h.

To characterize Rhod-SP@MSN-CD for labeling lysosomes, a lysosome tracker, LysoTracker Green, was used as the standard lysosome marker. HeLa cells were incubated with 50 μg/mL Rhod-SP@MSN-CD in culture medium for 3.0 h. To stain lysosomes, the cells were incubated with the indicated concentrations of LysoTracker Green 1.0 μM for 30 min before imaging. (Rhod-SP@MSN-CD channel: λ_{ex} = 559 nm, λ_{em} = 570−600 nm bandpass. LysoTracker Green channel: λ_{ex} = 488 nm, λ_{em} = 505−530 nm bandpass. Yellow: co-localization of red and green fluorescence).

Transmission Electron Microscopy Analysis. HeLa cells were treated with Rhod-SP@MSN-CD in media for 3.0 h at 37 °C. After washing with PBS, the cells were detached and centrifuged. The cell pellets were fixed with 2.5% glutaraldehyde in 0.1 M phosphate buffer for 2.5 h, dehydrated using an ascending alcohol series (20%, 40%, 60%, 80%, and 100% twice) for 20 min for each change, and then embedded in Araldite resin at 65 °C overnight. A 70 nm section was placed on a TEM grid and stained with saturated uranyl acetate and 0.2% Reynolds lead citrate before TEM imaging. Images were collected using a JEOL 1200 EXII scanning and transmission electron microscope (Japan Electron Optics Laboratory, Peabody, MA).

The Binding Specificity of Rhod-SP@MSN-CD-RGD. The binding specificity of Rhod-SP@MSN-CD-RGD to HeLa cells was performed using confocal laser scanning microscopy. MCF-7 cells were used as a negative control. HeLa cells and MCF-7 cells were seeded in cell culture dishes at a density of 4 × 10^4 cells/dish in RPMI 1640 medium with 15% fetal calf serum and allowed to grow for 2 days. The HeLa and MCF-7 cells were respectively incubated with Rhod-SP@MSN-CD-RGD (50 μg/mL) in culture medium with different incubation times.

RESULTS AND DISCUSSION

To reliably acquire signals activated by Cu^{2+} under acidic lysosomal environment (pH = 4.0−6.0), a rhodamine-−piropyran fluorescent probe, termed Rhod-SP, that recognizes the presence of lysosomal Cu^{2+} and then binds with it through spiropyran-based proton activation was designed and synthesized (see Scheme 1A, as well as Figures S1−S4 in the Supporting Information). Rhod-SP possessed a spiropyran recognition unit, which is a well-known metastable system susceptible to the activation of UV light or protonation,[33,34] and a latent fluorescent signal transduction unit of rhodamine. Rhod-SP can be activated by acidic pH to release the ligating phenolic group required for binding Cu^{2+} via collaborative coordination with C═O and C═N that promotes rhodamine ring-opening and shows a "switched on" fluorescence signal (see Scheme 1B). However, the fluorescent signal was silent when Rhod-SP was allowed into an alkaline environment. Next, to confer the probe with the ability to accumulate in lysosomes and, at the same time, bypass interference and degradation, we used mesoporous silica nanoparticles (MSNs) as a protective nanocoating, entrapping the probe in MSN channels. Meanwhile, MSNs were conjugated with β-cyclodextrin (β-CD) as a gatekeeper,[35,36] to eliminate interference from intracellular species, but allow Cu^{2+} ions to enter the nanopores and react with Rhod-SP. By their nanosize, MSNs are expected to internalize into cells by endocytosis and mainly accumulate in lysosomes.[26,29,30] Finally, to enhance cell specificity, β-CD was modified with a targeting vector peptide cyclo(Arg-Gly-Asp-Phe-Lys(mpa))[31] conjugated with adamantane (denoted as Ad-RGD) on β-CD via host−guest interactions of β-CD and Ad (see Scheme 2A). This Ad-RGD, when incorporated as a component with Rhod-SP@MSN-CD, exhibited specific cell binding to $\alpha_v\beta_3$ and $\alpha_v\beta_5$ integrin receptors overexpressed on the membrane of most cancer cells, thereby improving internalization efficiency of the nanoprobe through receptor-mediated endocytosis (Scheme 2B). The newly designed nanoprobe not only makes full use of the acidic pH environment to activate the probe, but also inhibits the macromolecules of proteins and enzymes from diffusing into the nanopores to degrade the chemical probe, which allows one to track in a location-specific manner and visualize lysosomal Cu^{2+} with high spatial resolution.

Scheme 2. (A) Synthetic Route of Rhod-SP@MSN-CD-RGD. (B) Schematic Illustration of the Nanoprobe Rhod-SP@MSN-CD-RGD for Cu^{2+} Imaging in Lysosomes

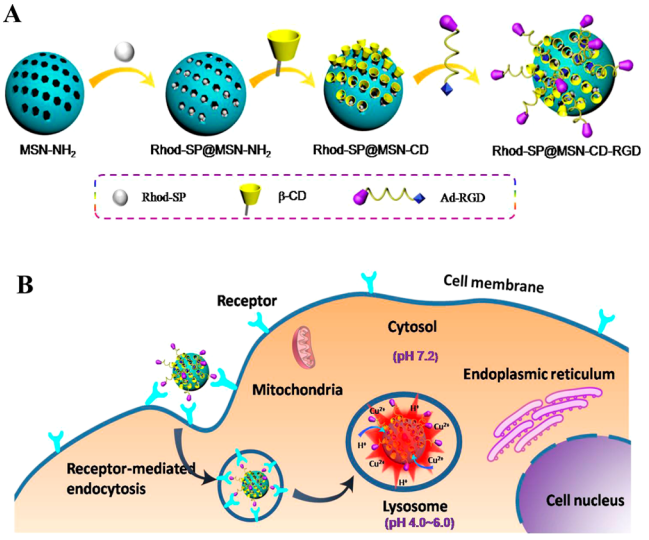

Figure S5 and Figure 1A show the absorption and fluorescence spectra of Rhod-SP. At pH 8.0, Rhod-SP exhibited no absorption in the visible region and was essentially nonfluorescent, because of the dual closure of rhodamine and spiropyran moieties. Upon the addition of Cu^{2+}, no significant change in absorption or fluorescence was noted, indicating that the spirolactam moiety of Rhod-SP remained intact. In an acidic medium (pH 5.0), however, the absorption spectra of Rhod-SP showed a significant band at 400−460 nm, which could be ascribed to the protonated merocyanine form of spiropyran, but, still, no characteristic absorption of the rhodamine moiety was observed. However, upon the addition of Cu^{2+}, an absorption at 550 nm emerged concomitant with a fluorescent emission at 590 nm, indicating Cu^{2+}-induced rhodamine ring-opening via metal-mediated coordination reaction in an acidic medium.[37] The inset of Figure 1A, and Figure S6 in the Supporting Information, further confirmed the pH dependence of Rhod-SP for Cu^{2+} sensing. Furthermore, an increase of fluorescence with increasing Cu^{2+} concentration was observed over the pH range of 4.0−6.0, which corresponds to the acidic pH microenvironment in lysosomes.[22]

dx.doi.org/10.1021/ac503240x | Anal. Chem. XXXX, XXX, XXX−XXX

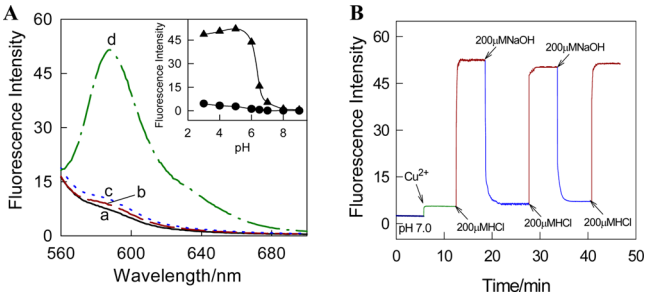

Figure 1. (A) Fluorescence emission spectra (λ_{ex} = 550 nm) of Rhod-SP under different conditions: (a), 1.0 μM Rhod-SP in 50% buffer−CH_3CN (v/v) solution (pH 7.0); (b) the solution described for that in panel a, + 10.0 μM Cu^{2+}; (c) 1.0 μM Rhod-SP in 50% buffer-CH_3CN (v/v) solution (pH 5.0); and (d) the soluton described for panel c + 10.0 μM Cu^{2+}. Inset shows the effect of pH on the fluorescence emission of Rhod-SP in the absence (●) and presence (▲) of 10.0 μM Cu^{2+}. (B) Real-time fluorescence records ($\lambda_{ex}/\lambda_{ex}$ = 550 nm/590 nm) of Rhod-SP upon addition of Cu^{2+} in 50% buffer−CH_3CN solution (pH 7.0), following several repeated concentration step changes between 200 μM HCl solution and then 200 μM NaOH solution.

Next, the binding mode between Rhod-SP and Cu^{2+} was verified by ^1H NMR analysis (see Figure S7 in the Supporting Information). The peaks at δ 12.60 and 9.18 ppm for the two protons (OH, N═CH) disappeared after the addition of Cu^{2+}, implicating that nitrogen and oxygen take part in Cu^{2+} binding. In addition, other peaks for the active protons broadened by the increase of proton exchange, and both the peaks shifted upfield because of the electron-deshielding effect of Cu^{2+} on them. From the ESI-MS spectrum (Figure S8 in the Supporting Information), a new m/z peak was found to be 863.82 in its ESI-MS upon addition of Cu^{2+}, which was assigned to [Rhod-SP + Cu^{2+}]$^+$. The $(A - A_0)/A_0$ value displayed a maximum at a molar fraction of ~0.508 by Job's method in Figure S9 in the Supporting Information, indicating a 1:1 stoichiometry of Cu^{2+} to Rhod-SP in the complex, where A_0 and A represent the absorbance at 550 nm of Rhod-SP without or with Cu^{2+}, respectively.

As shown in Figure 1B, further investigation revealed rapid and complete reversibility of the response of Rhod-SP to Cu^{2+} with pH changes. A slight increase in fluorescence intensity at 590 nm could be observed upon the addition of Cu^{2+} in neutral solution, but a strong fluorescence was realized at acidic pH. Importantly, fluorescence could be "switched off" at alkaline pH, indicating that Rhod-SP could be exploited for the real-time monitoring of Cu^{2+} in a complex intracellular environment. Collectively, these *in vitro* results demonstrated that the Rhod-SP fluorescence signal could reversibly become quenched in cytoplasm, but, conversely, it would be illuminated in acidic subcellular organelles, such as endosome or lysosome.

Selectivity is another important parameter by which to assess the performance of a fluorescent probe in a complex cell environment. At pH 5.0 (see Figure S10 in the Supporting Information), the fluorescence intensity of Rhod-SP displayed negligible variation in the presence of K^+, Na^+, Mg^{2+}, Ca^{2+}, Zn^{2+}, Fe^{2+}, Fe^{3+}, Hg^{2+}, Cr^{3+}, Cd^{2+}, Pb^{2+}, and Cl^-, SO_4^{2-}, as well as aspartic acid (Asp), glutamic acid (Glu), ATP, glucose, and β-glucosidase (β-GCD). However, the strong fluorescence caused by Cu^{2+} weakened rapidly upon addition of biological thiols, such as cysteine (Cys), glutathione (GSH), bovine serum albumin (BSA), and Caspase-1 (see Figure S11 in the Supporting Information), primarily because of the strong binding between the sulfhydryl function and Cu^{2+}. These results suggested that free Rhod-SP for Cu^{2+} detection would be severely thwarted by interference from complex biological systems.

Based on the above results, it can be inferred that Rhod-SP would be a good lysosome-activatable Cu^{2+} probe. However, to protect Rhod-SP from degradation and interference by the physiological environment, we engineered Rhod-SP on mesoporous silica nanoparticles (MSNs) as a protective nanocoat entrapping Rhod-SP molecules in MSNs channels (Rhod-SP@MSN). The surface of MSNs was then functionalized with a β-cyclodextrin (β-CD) as a gatekeeper to cap the pores and enhance the dispersibility and inertness of MSNs in aqueous media (see Scheme 2A). MSN-NH_2 was prepared according to protocols described in the literature.[34] Transmission electron microscopy (TEM) and powder X-ray diffraction (PXRD) confirmed the well-ordered structures with typical MCM-41 hexagonal arrangements, having an approximate diameter of 80 nm (Figure 2). Using a diffusion

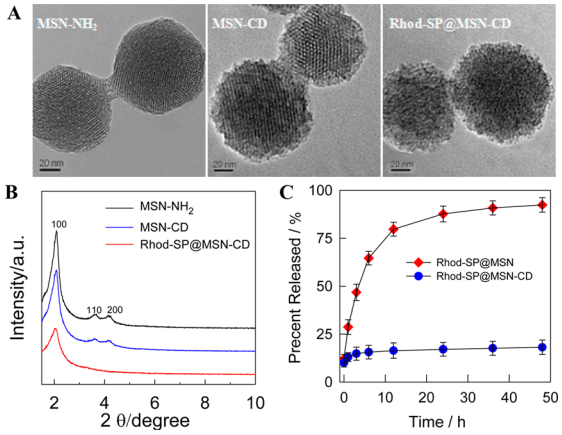

Figure 2. (A) TEM images and (B) small-angle powder XRD patterns of MSN-NH_2, MSN-CD, and Rhod-SP@MSN-CD. (C) The cumulative release profiles of Rhod-SP from Rhod-SP@MSN and Rhod-SP@MSN-CD in buffer solution (20 mM, pH 5.0) containing 10.0 μM Cu^{2+} at 37 °C.

protocol, Rhod-SP molecules were entrapped in MSN-NH_2. β-CD was installed on the Rhod-SP-loaded MSN surface via the amidation reaction between MSN-NH_2 and mono(6-(*p*-toluenesulfonyl))permethylated β-cyclodextrin (β-CD) (denoted as Rhod-SP@MSN-CD). The loading efficiency of Rhod-SP in MSN-CD was estimated to be ~12 wt %. The treatment processes of the MSNs were characterized using TEM, PXRD, the zeta potential, and nitrogen adsorption−desorption isotherms. From Figure 2A, the average diameter of MSN-CD and Rhod-SP@MSN-CD showed no significant differences from that of MSN-NH_2. However, while an obvious border was observed around the treated MSN-CD, XRD patterns showed that the low-angle reflections indexed as (110) and (200) disappeared after loading with Rhod-SP, because of an effect from the filled pores (Figure 2B). In addition, nitrogen adsorption−desorption isotherms showed the typical Type IV curves with a surface area of 693 m^2 g^{-1} and an average pore size of 2.8 nm of MSN-NH_2, but the surface area and pore size decreased with increasing surface density and infilling (Figure S12 in the Supporting Information). The zeta potential values of MSN-NH_2, MSN-CD, and Rhod-SP@MSN-CD were +37.5,

dx.doi.org/10.1021/ac503240x | *Anal. Chem.* XXXX, XXX, XXX−XXX

+14.2, and +27.8 mV, respectively (see Figure S13 in the Supporting Information). Furthermore, Fourier transform infrared (FTIR) spectroscopy (see Figure S14 in the Supporting Information) and ^{13}C CP-MAS solid-state NMR spectroscopy provided solid evidence for the successful functionalization of MSNs with β-CD rings (Figure S15 in the Supporting Information). Therefore, Rhod-SP molecules were effectively entrapped in MSNs without being released for more than 48 h (Figure 2C). Nonetheless, Cu^{2+} could freely diffuse into the inner mesopores through the cavities of the β-CD rings to react with Rhod-SP (see Figure S16 in the Supporting Information). Figure S17 in the Supporting Information shows that the uniformly distributed MSN-CD exhibited an improved long-term stability in cell culture medium, which was mainly attributed to the enhanced water-solubility after conjugating with β-CD. It was worth noting that the wavelength of maximum emission showed a slight blue shift from 590 nm to 575 nm, but no observable change in absorption spectra upon loading Rhod-SP into the hydrophobic inner mesopores (see Figure S18 in the Supporting Information).

Figure 3A shows fluorescence spectra changes of Rhod-SP@MSN-CD in response to different concentrations of Cu^{2+}. The addition of increasing concentrations of Cu^{2+} to the aqueous solution of Rhod-SP@MSN-CD at pH 5.0 elicited a dramatic

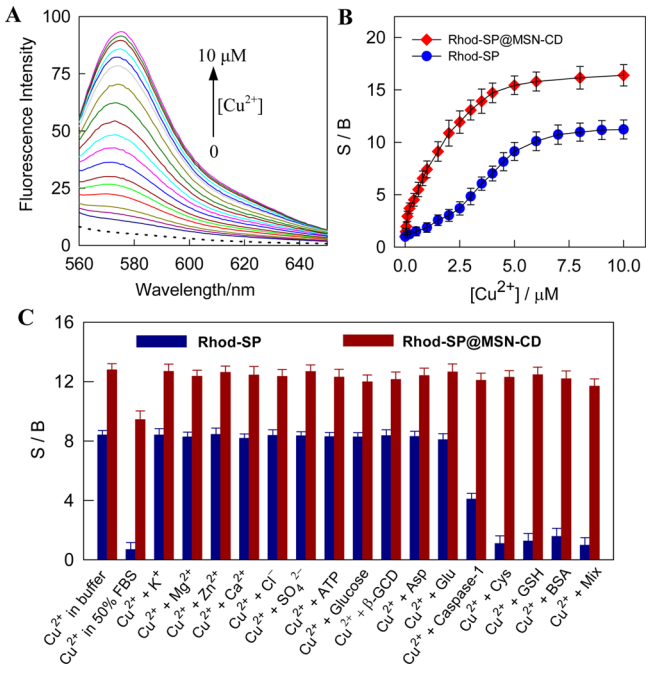

Figure 3. (A) Fluorescence emission spectra of Rhod-SP@MSN-CD (λ_{ex} = 550 nm) in the presence of different concentrations of Cu^{2+} in buffer solution (20 mM, pH 5.0). The arrows indicate the change in signal observed as the Cu^{2+} concentration increases (0.05, 0.1, 0.2, 0.4, 0.6, 0.8, 1.0, 1.5, 2.0, 2.5, 3.0, 3.5, 4.0, 5.0, 6.0, 8.0, and 10.0 μM). Dotted line represents the fluorescence spectrum of buffer solution. (B) S/B of Rhod-SP@MSN-CD, as a function of Cu^{2+} concentration. (C) S/B of Rhod-SP (1.0 μM, red bars) and Rhod-SP@MSN-CD (50 μg/mL, blue bars) to Cu^{2+} (50.0 μM) in buffer solution, in 50% FBS, and in the presence of possible competitors (K^+, Mg^{2+}, Zn^{2+}, Ca^{2+}/50.0 μM, Cl^-, SO_4^{2-}/100.0 μM, Asp, Glu, ATP, Cys, GSH, glucose/5.0 mM, BSA/0.1 mg/mL, and β-glucosidase (β-GCD), Caspase-1/5U, and a mixture containing all of the tested substances) in buffer solution.

enhancement of the emission intensity that covered 0 to 10.0 μM Cu^{2+}, and a signal-to-background ratio (S/B) of 16.8 was achieved in the presence of 5.0 μM Cu^{2+} (see Figure 3B); here, S/B is defined as

$$\mathrm{S/B} = \frac{F - F_{\mathrm{buffer}}}{F_0 - F_{\mathrm{buffer}}}$$

where F is the fluorescence intensity at 575 nm of Rhod-SP@MSN-CD with Cu^{2+}, F_0 the fluorescence intensity at 575 nm of Rhod-SP@MSN-CD without Cu^{2+}, and F_{buffer} the fluorescence intensity at 575 nm of Rhod-SP@MSN-CD with a buffer. There was good linearity between S/B and the concentrations of Cu^{2+} in the range of 0.1−4.0 μM. The detection limit based on 3σ/slope was estimated to be 1.26 nM, which exhibited higher sensitivity toward Cu^{2+} than that of free Rhod-SP (62.5 nM), as shown in Figure 3B (representative fluorescence spectra are shown in Figure S19 in the Supporting Information). This was most likely because the good hydrophobic environment offered by the nanopores could strengthen the interaction between Rhod-SP molecules and Cu^{2+}. Moreover, because of the protective effect of MSNs capped with β-CD, Rhod-SP@MSN-CD exhibited high stability and excellent anti-interference ability in complex biological samples (see Figure 3C, as well as Figure S20 in the Supporting Information).

Following characterization of the spectroscopic properties of Rhod-SP@MSN-CD, we sought to apply Rhod-SP@MSN-CD to image fluctuations in exchangeable copper pools in living cells. The cytotoxicity of both Rhod-SP and Rhod-SP@MSN-CD on living cells was first evaluated by employing standard cell viability protocols (MTT assay) (see Figure S21 in the Supporting Information). After culturing HeLa cells with Rhod-SP and Rhod-SP@MSN-CD for 24 h, their cellular viability was over 95%, and no significant difference in morphology was observed, even when the concentration was increased up to 10.0 μM Rhod-SP or 100 μg/mL Rhod-SP@MSN-CD. Next, Rhod-SP@MSN-CD was used for confocal imaging experiments to further verify its ability to detect intracellular exchangeable copper using HeLa cells as a model cell line. As shown in Figure 4, and in Figure S22 in the Supporting Information, HeLa cells showed no detectable fluorescence signals without the addition of $CuCl_2$ (Figure 4a), but strong fluorescence could be visualized when they were pretreated with exogenous $CuCl_2$ (Figure 4b). Moreover, we observed a tendency toward increased fluorescence with increasing concentrations of $CuCl_2$ (see Figure S23 in the Supporting Information). However, when $CuCl_2$-supplemented cells (Figure 4b) were further treated with the reducing reagent ascorbate to globally deplete intracellular Cu^{2+} stores, the fluorescence completely disappeared, essentially because ascorbate is known to change the redox equilibrium to promote the reduction of Cu^{2+} to Cu^+ (Figure 4c).[38] We further investigated fluorescence change caused by endogeneous Cu^{2+} by treating HeLa cells with pyrrolidine dithiocarbamate (PDTC), the precursor for promoting oxidation of glutathione to increase the intracellular level of Cu^{2+} ions.[39] Compared with the results shown in Figure 4a, it can be seen in Figure 4d that a weak fluorescence signal is emitted from PDTC-treated cells. These results can be interpreted to mean that changes in both exogenous and endogeneous Cu^{2+} can be monitored by Rhod-SP@MSN-CD. Since Rhod-SP selectively responded to the coexistence of H^+ and Cu^{2+} *in vitro*, it could be hypothesized

dx.doi.org/10.1021/ac503240x | *Anal. Chem.* XXXX, XXX, XXX−XXX

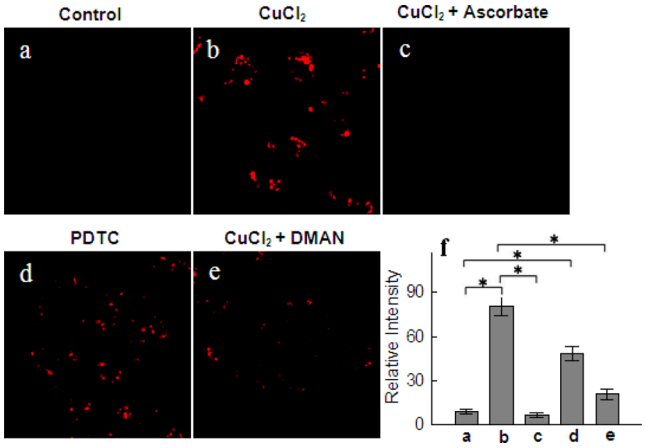

Figure 4. Confocal microscopy images of HeLa cells using Rhod-SP@MSN-CD under different conditions: (a) cells incubated with Rhod-SP@MSN-CD (50 μg/mL) for 3.0 h; (b) cells supplemented with 50 μM $CuCl_2$ for 12.0 h and then incubated with Rhod-SP@MSN-CD (50 μg/mL) for 3.0 h; (c) cells from panel (b), treated with 1.0 mM ascorbate for 2.0 h; (d) cells from panel (a), treated with 100 μM PDTC for 2.0 h; and (e) cells from panel (b), treated with a proton sponge of DMAN for 2.0 h (λ_{ex} = 559 nm; λ_{em} = 570−600 nm). (f) Graph showing quantification of mean fluorescence intensity of each condition (a−e), normalized to the control condition. Statistical analyses were performed with a two-tailed Student's *t*-test. Asterisk (*) indicates $P < 0.05$ (n = 3), and error bars are ±SD (SD = standard deviation).

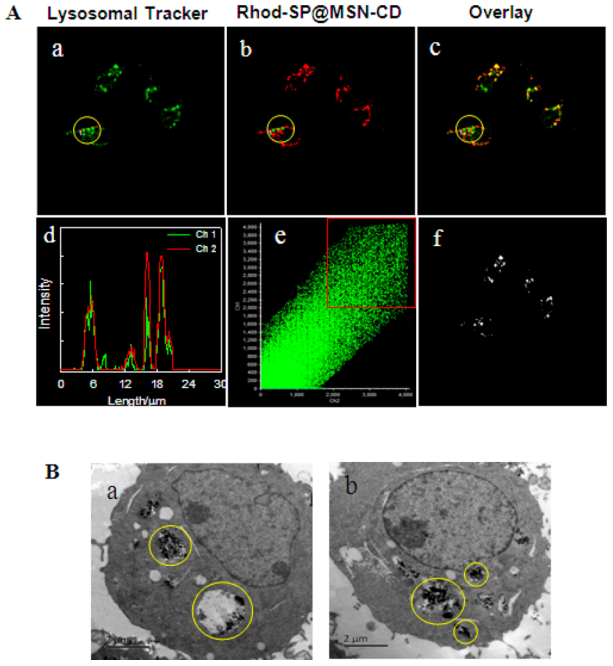

Figure 5. (A) Rhod-SP@MSN-CD colocalizes to the lysosome in HeLa cells. Cells were stained with (a) 1.0 μM LysoTracker Green (Channel 1, λ_{ex} = 488 nm; λ_{em} = 505−530 nm) for 0.5 h at 37 °C, (b) 50 μg/mL Rhod-SP@MSN-CD (Channel 2, λ_{ex} = 559 nm; λ_{em} = 570−600 nm) with $CuCl_2$ (50.0 μM) for 3.0 h at 37 °C, (c) overlay of panels a and b, (d) intensity profile of region of interest (ROI) across the HeLa cell, (e) intensity scatter plot of LysoTracker Green and Rhod-SP@MSN-CD, and (f) simulated image (the white pixels, as represented by the scatter plot shown in panel e, were highlighted by selecting the points within the noted red rectangular region). (B) TEM micrographs of HeLa cells incubated with (a) MSNs and (b) Rhod-SP@MSN-CD for 3.0 h.

that the intracellular response behavior of Rhod-SP@MSN-CD happened in the acidic lysosomal microenvironment rather than the cytoplasm or other organelles with neutral environments. To demonstrate this proposition, HeLa cells were treated with 1,8-bis(dimethylamino)naphthalene (DMAN), a common proton sponge, to promote lysosomal damage.[40] From Figure 4e, an obvious decrease in fluorescence was observed in these cells from the proton-sponge effect, leading to the successful escape of Rhod-SP@MSN-CD into the cytoplasm, preliminarily proving that the fluorescence enhancement of Rhod-SP@MSN-CD was dependent on lysosomal acidity. Fluorescence imaging analysis convincingly proved that the cells could only be illuminated by Rhod-SP@MSN-CD in the simultaneous presence of Cu^{2+} and lysosomal protons.

As expected, Rhod-SP@MSN-CD displayed well-localized fluorescence within lysosomes. HeLa cells were co-stained with Rhod-SP@MSN-CD for 3.0 h in the presence of exogenous Cu^{2+} and LysoTracker Green for 5 min at 37 °C. As shown in Figure 5A (panels (a)−(c)), the fluorescent images between Rhod-SP@MSN-CD and LysoTracker Green overlapped very well. The intensity profiles of the linear regions of interest across HeLa cells stained with Rhod-SP@MSN-CD and LysoTracker also tended toward synchronization (panel (d) in Figure 5A). From the intensity correlation plots (panel (e) in Figure 5A), a high Pearson's colocalization coefficient of 0.942 and overlap coefficient of 1.626 were obtained, respectively, and the white pixels (Figure 5Af) identified those lysosomes with high-intensity distribution of the two dyes. The results indicated that Rhod-SP@MSN-CD was specifically accumulated in lysosomes and activated by the coexistence of acidic pH and Cu^{2+}. To provide additional physical evidence for subcelluar residence of nanoprobe, TEM analysis was applied to image the cell uptake of MSNs and Rhod-SP@MSN-CD. From Figure 5B, it can be clearly seen that both were internalized by cells and trapped inside lysosomes. The superior colocalization results can be attributed to two factors. First, the MSNs could forwardly accumulate into lysosomes after internalizing into cells by endocytosis. Second, the acidic lysosomal environment could effectively activate Rhod-SP to function a good response to Cu^{2+}. Thus, Rhod-SP@MSN-CD exhibits excellent spatiotemporal resolution capability for specifically sensing lysosomal Cu^{2+}.

Since β-CD on the surface of Rhod-SP-loaded MSNs confers the capability of nanoparticles to further conjugate with various functional receptors, a guiding unit of c(RGDyK) peptide conjugated adamantane (Ad-RGD) as prototypical system was incorporated on the surface of Rhod-SP@MSN-CD by host−guest interactions of β-CD and Ad to enhance cell specificity (see Scheme 2). The characteristics confirmed that c(RGDyK) peptide was well-modified on the surface of MSNs. After conjugation of Rhod-SP@MSN-CD with Ad-RGD peptide, the zeta potential of the nanoprobes changed from +27.8 mV of Rhod-SP@MSN-CD to +6.6 mV of Rhod-SP@MSN-CD-RGD (Figure S24 in the Supporting Information). The dynamic light scattering (DLS) analysis also indicated that diameter of the obtained nanoprobes changed from ∼80 nm of Rhod-SP@MSN-CD to ∼98 nm of Rhod-SP@MSN-CD-RGD with excellent dispersion (Figure S25 in the Supporting Information). Moreover, FTIR spectroscopy gave direct evidence, because of the emerging absorption bands of acylamide vibration and carboxyl stretching vibration at 1541 and 1670 cm^{-1}, respectively (Figure S26 in the Supporting Information).

dx.doi.org/10.1021/ac503240x | *Anal. Chem.* XXXX, XXX, XXX−XXX

Then, the cell specificity of Rhod-SP@MSN-CD-RGD was verified using flow cytometry and confocal imaging experiments by incubating the probe with HeLa cells and MCF-7 cells, respectively. Flow cytometry experiments (Figure S27 in the Supporting Information) in HeLa cells revealed a marked shift in population distribution from low fluorescence intensity to high fluorescence intensity when the cells were supplemented with Cu^{2+}. This response can be ascribed to the high affinity between the cyclic RGD peptide and both $\alpha_v\beta_3$ and $\alpha_v\beta_5$ integrins,[41] which are expressed at high levels on HeLa cells, but at lower levels on MCF-7 cells, in turn, leading to enhanced endocytosis of the nanoprobe. Subsequent analysis using confocal imaging further confirmed that receptor mediation conferred efficient endocytosis. Significant fluorescence was clearly visualized in HeLa cells after being incubated with Rhod-SP@MSN-CD-RGD for 30 min (see Figures S28A and S28B in the Supporting Information), and high colocalization between Rhod-SP@MSN-CD-RGD and LysoTracker was seen in lysosomes, but only a weak fluorescent signal was observed in MCF-7 cells, even if the incubation time reached 3.0 h (see Figures S28C and S28D in the Supporting Information). Moreover, TEM confirmed that Rhod-SP@MSN-CD-RGD exhibited a higher uptake efficiency into HeLa cells and faster lysosomal accumulation (30 min) than that of MSNs and Rhod-SP@MSN-CD (see Figure S29 in the Supporting Information). Clearly, the presence of RGD peptides on the surface of nanoprobes conferred both targeting and internalization properties to specific cell populations.

Finally, we evaluated the potential application of Rhod-SP@MSN-CD-RGD in the diagnosis and evaluation of Cu^{2+}-related diseases by incubating Rhod-SP@MSN-CD-RGD with live human normal liver cells (HL-7702) and human hepatoma cells (HepG2). Figure S30 in the Supporting Information clearly shows that the fluorescence of HepG2 was apparently brighter than HL-7702, indicating that the content of Cu^{2+} inside the lysosomes of hepatoma cells is higher than that of normal liver cells, consistent with previous studies.[18,42] Thus, Rhod-SP is not only useful for the imaging lysosomal Cu^{2+} on the cellar level, but it is also valuable for disease diagnosis. In the latter case, the nanoprobe was able to detect the Cu^{2+} level in lysosomes, suggesting the development of liver injury in living cells.

CONCLUSIONS

In summary, a dual Cu^{2+}- and proton-activated fluorescent nanoprobe has been developed to monitor Cu^{2+} in lysosomes. To the best of our knowledge, such a dual-locked model system that activates the probe's fluorescence by both the target analyte and the specific location remains essentially undeveloped; thus, the approach woud successfully address the challenges of intracellular analysis. First, selective accumulation and subsequent fluorescence activation eliminate false signals and improve spatial resolution and sensitivity. Second, the encapsulation of functional probe molecules into nanopores effectively protects the probes' stability and, at the same time, avoids interference from complex biological environments. Finally, modification with β-CD on the surface of mesoporous silica nanoparticles (MSNs) not only dramatically improved the nanoprobe's stability and biocompatibility in the physiological environment, but also conferred the capability of the nanoprobe to further conjugate with various functional receptors, which makes the nanoprobe possess dual-targetable ability. This is a flexible and universal design strategy for lysosome-targeted chemical probes by simply changing the target recognition element, hence making it applicable to other analytes of interest.

ASSOCIATED CONTENT

Supporting Information

More experimental details and additional spectroscopic data as noted in text. This material is available free of charge via the Internet at http://pubs.acs.org.

AUTHOR INFORMATION

Corresponding Author

*Fax: +86-731-8882 2523. E-mail: Yangrh@hnu.edu.cn.

Author Contributions

§These authors contributed equally to this work.

Notes

The authors declare no competing financial interest.

ACKNOWLEDGMENTS

The authors acknowledge financial support through the National Natural Science Foundation of China (Nos. 21305036, 21135001, and J1103312), the Foundation for Innovative Research Groups of NSFC (No. 21221003), the "973" National Key Basic Research Program (No. 2011CB91100-0), Hunan Provincial Natural Science Foundation of China (No. 2015JJ3035), and the Fundamental Research Funds for the Central Universities.

REFERENCES

(1) *Principles of Bioinorganic Chemistry*; Lippard, S. J., Berg, J. M., Eds.; University Science Books: Mill Valley, CA, 1994.

(2) Prohaska, J.; Gybina, A. A. *J. Nutr.* **2004**, *134*, 1003−1006.

(3) Culotta, V. *J. Biol. Inorg. Chem.* **2010**, *15*, 1−2.

(4) Strausak, D.; Mercer, J. F. B.; Dieter, H. H.; Stremmel, W.; Multhaup, G. *Brain Res. Bull.* **2001**, *55*, 175−185.

(5) Oyama, F.; Murakami, N.; Ihara, Y. *Neurosci. Res.* **1998**, *31*, 1−8.

(6) Van den Berghe, P. V. E.; Folmer, D. E.; Malingre, H. E. M.; Van Beurden, E.; Klomp, A. E. M.; De Sluis, B. V.; Merkx, M.; Berger, R.; Klomp, L. W. J. *Biochem. J.* **2007**, *407*, 49−59.

(7) Zietz, B. P.; de Vergara, J. D.; Dunkelberg, H. *Environ. Res.* **2003**, *92*, 129−138.

(8) Lutsenko, S.; Gupta, A.; Burkhead, J. L.; Zuzel, V. *Arch. Biochem. Biophys.* **2008**, *476*, 22−32.

(9) (a) Gaggelli, E.; Kozlowski, H.; Valensin, D.; Valensin, G. *Chem. Rev.* **2006**, *106*, 1995−2044. (b) Bertini, I.; Rosato, A. *Cell. Mol. Life Sci.* **2008**, *65*, 89−91.

(10) Kaler, S. G. *Nat. Rev. Neurol.* **2011**, *7*, 15−29.

(11) For reviews, see: (a) Que, E. L.; Domaille, D. W.; Chang, C. J. *Chem. Rev.* **2008**, *108*, 1517−1549. (b) Que, E. L.; Chang, C. J. *Chem. Soc. Rev.* **2010**, *39*, 51−60. (c) Domaille, D. W.; Que, E. L.; Chang, C. J. *Nat. Chem. Biol.* **2008**, *4*, 168−175.

(12) Jung, H. S.; Kwon, P. S.; Lee, J. W.; Kim, J. I.; Hong, C. S.; Kim, J. W.; Yan, S.; Lee, J. Y.; Lee, J. H.; Joo, T.; Kim, J. S. *J. Am. Chem. Soc.* **2009**, *131*, 2008−2012.

(13) You, Y.; Han, Y.; Lee, Y. M.; Park, S. Y.; Nam, W.; Lippard, S. J. *J. Am. Chem. Soc.* **2011**, *133*, 11488−11491.

(14) Hirayamaa, T.; Van de Bittner, G. C.; Gray, L. W.; Lutsenko, S.; Chang, C. J. *Proc. Natl. Acad. Sci. U.S.A.* **2012**, *109*, 2228−2233.

(15) Zhu, A.; Qu, Q.; Shao, X.; Kong, B.; Tian, Y. *Angew. Chem., Int. Ed.* **2012**, *51*, 7185−7189.

(16) Dodani, S. C.; Leary, S. C.; Cobine, P. A.; Winge, D. R.; Chang, C. J. *J. Am. Chem. Soc.* **2011**, *133*, 8606−8616.

(17) Wang, X.; Ma, X.; Yang, Z.; Zhang, Z.; Wen, J.; Geng, Z.; Wang, Z. *Chem. Commun.* **2013**, *49*, 11263−11265.

(18) Li, P.; Zhou, H.; Tang, B. *J. Photochem. Photobiol., A* **2012**, *249*, 36−40.
(19) Masanta, G.; Lim, C. S.; Kim, H. J.; Han, J. H.; Kim, H. M.; Cho, B. R. *J. Am. Chem. Soc.* **2011**, *133*, 5698−5700.
(20) Chen, Y.; Zhu, C.; Yang, Z.; Chen, J.; He, Y.; Jiao, Y.; He, W.; Qiu, L.; Cen, J.; Guo, Z. *Angew. Chem., Int. Ed.* **2013**, *52*, 1688−1691.
(21) Repnik, U.; Turk, B. *Mitochondrion* **2010**, *10*, 662−669.
(22) Luzio, J. P.; Pryor, P. R.; Bright, N. A. *Nat. Rev. Mol. Cell Biol.* **2007**, *8*, 622−632.
(23) Shao, N.; Jin, J. Y.; Cheung, S. M.; Yang, R. H.; Chan, W. H.; Mo, T. *Angew. Chem., Int. Ed.* **2006**, *45*, 4944−4948.
(24) Shao, N.; Jin, J. Y.; Wang, H.; Zheng, J.; Yang, R. H.; Chan, W. H.; Abliz, Z. *J. Am. Chem. Soc.* **2010**, *132*, 725−736.
(25) Shao, N.; Wang, H.; Gao, X. D.; Yang, R. H.; Chan, W. H. *Anal. Chem.* **2010**, *82*, 4628−4636.
(26) (a) Lu, J.; Liong, M.; Li, Z.; Zink, J. I.; Tamanoi, F. *Small* **2010**, *6*, 1794−1805. (b) Vivero-Escoto, J. L.; Slowing, I. I.; Trewyn, B. G.; Lin, V. S. *Small* **2010**, *6*, 1952−1967.
(27) Li, Z.; Barnes, J. C.; Bosoy, A.; Stoddart, J. F.; Zink, J. I. *Chem. Soc. Rev.* **2012**, *41*, 2590−2605.
(28) Tarn, D.; Ashley, C.; Xue, M.; Carnes, E.; Zink, J. I.; Brinker, C. J. *Acc. Chem. Res.* **2013**, *46*, 792−801.
(29) Rivera-Gil, P.; Vazquez-Vazquez, C.; Giannini, V.; Callao, M. P.; Parak, W. J.; Correa-Duarte, M. A.; Alvarez-Puebla, R. A. *Angew. Chem., Int. Ed.* **2013**, *52*, 13694−13698.
(30) Wu, X.; Li, Z.; Yang, L.; Han, J.; Han, S. *Chem. Sci.* **2013**, *4*, 460−467.
(31) Arap, W.; Pasqualini, R.; Ruoslahti, E. *Science* **1998**, *279*, 377−380.
(32) Kresge, C. T.; Leonowicz, M. E.; Roth, W. J.; Vartuli, J. C.; Beck, J. S. *Nature* **1992**, *359*, 710−712.
(33) Berkovic, G.; Krongauz, V.; Weiss, V. *Chem. Rev.* **2000**, *100*, 1741−1754.
(34) Raymo, F. M.; Giordani, S. *J. Am. Chem. Soc.* **2001**, *123*, 4651−4652.
(35) Park, C.; Lee, K.; Kim, C. *Angew. Chem., Int. Ed.* **2009**, *48*, 1275−1278.
(36) Luo, Z.; Cai, K.; Hu, Y.; Zhao, L.; Liu, P.; Duan, L.; Yang, W. *Angew. Chem., Int. Ed.* **2011**, *50*, 640−643.
(37) Zhao, Y.; Zhang, X. B.; Han, Z. X.; Qiao, L.; Li, C. Y.; Jian, L. X.; Shen, G. L.; Yu, R. Q. *Anal. Chem.* **2009**, *81*, 7022−7030.
(38) Harris, E. D.; Percival, S. S. *Am. J. Clin. Nutr.* **1991**, *54*, 1193S−1197S.
(39) Verhaegh, G. W.; Richard, M.; Hainaut, P. *Mol. Cell. Biol.* **1997**, *17*, 5699−5706.
(40) Alder, R. W.; Bowman, P. S.; Steele, W. R. S.; Winterman, D. R. *Chem. Commun.* **1968**, 723−724.
(41) Chen, X. Y.; Conti, P. S.; Moats, R. A. *Cancer Res.* **2004**, *64*, 8009−8014.
(42) Ralle, M.; Huster, D.; Vogt, S.; Schirrmeister, W.; Burkhead, J. L.; Capps, T. R.; Gray, L.; Lai, B.; Maryon, E.; Lutsenko, S. *J. Biol. Chem.* **2010**, *285*, 30875−30883.